Perception sensor evaluation: LiDAR capability in the presence of dust

Perception sensor evaluation: LiDAR capability in the presence of dust

J.C.D. van Zundert
0677177

CST 2013.101

Traineeship report

Coach: T.G. Phillips (University of Queensland)

Supervisor: prof. R. McAree (University of Queensland)
prof.dr.ir. M. Steinbuch

Eindhoven University of Technology
Department of Mechanical Engineering
Control Systems Technology

Eindhoven, November 5, 2013

Contents

Chapter 1

Introduction

The mining industry is a primary industry in Australia and is still an important research area. A particular aspect of the current research focusses on the automation of the mining process. For example, autonomous digging or loading of haul trucks. In order to do so, the machines have to be equipped with sensing capability. Where humans mainly use their eyes, these machines can be equipped with lasers for perception tasks. Light Detecting And Ranging (LiDAR) sensors are commonly used in mining automation but have limited reliability and robustness when atmospheric obscurants such as dust are present. The interference with such particles can result in spurious returns or even no returns at all. As large equipment and humans are involved, the demand for robustness and reliability is high in the mining industry.

The aim of this project is to study the qualitative behaviour of four different LiDAR sensors with respect to dust. The outcome should allow for enhancements in the usage of LiDAR sensors in mining environments. Therefore, the operational boundaries, capabilities and limitations of the LiDAR sensors are studied with respect to dust.

The following four LiDAR scanners were evaluated:

- SICK LD-LRS3100,
- SICK LD-MRS400102,
- SICK LMS511-10100 PRO, and
- Velodyne HDL-64E S2.

An experimental setup was created which allows for conducting repeatable experiments with adjustable and measurable dust clouds. The short range tests focused on sensor behaviour as the dust cloud width was varied from $2m$ to $5m$ and are presented in [1]. This report focuses on sensor behaviour as the range to the target wall is varied from $10m$ to $25m$ in $5m$ increments. The width of the dust cloud in these tests was kept constant at $5m$.

The contents of this report are as follows. In Chapter 2 the basic principle of LiDAR sensors is explained as well as their interference with dust. Furthermore, the sensor specific capabilities are discussed for the four sensors used in this project. The experimental setup and procedure are described in Chapter 3 and in Chapter 4 the results are presented. The final chapter, Chapter 5, contains recommendations for future research.

Chapter 2

Light Detecting And Ranging sensors

2.1 Basic principle

Light Detecting And Ranging (LiDAR) sensors use the time of flight principle. In the most simple form a LiDAR sensor has a single static light emitter-detector pair. The emitter sends out light pulses of which, in case of diffuse reflection, some are reflected towards the detector. By measuring the time it takes between sending and receiving a light pulse and knowing the speed of the light, it can easily be determined what the distance was that the pulse has travelled. The range (the distance from the sensor to the detected object) is half this distance.

By repeating this principle at a high frequency and in multiple directions (for example by changing the orientation or using multiple emitter-detector pairs) it is possible to build a map of the surroundings in multiple dimensions.

Typically, a LiDAR sensor returns the orientation of the laser and the range (i.e. the estimated distance to the target). Using this information it can be determined where the target is with respect to the co-ordinate frame of the sensor. Besides reporting this information, each of the tested sensors reports additional data which is different between the sensors. After the following section, in which the interference with dust is discussed, each of the sensors are discussed in more detail.

2.2 Interference with dust

The interference between a LiDAR pulse and dust is described in this section.

Dust is basically a cloud of micrometre sized particles. LiDAR sensors use near-infrared light which has a wavelength outside the visible spectrum and is close to the size of the dust particles. All four sensors used in this study emit near-infrared light with a wavelength of approximately $905nm$. The possible behaviours when a near-infrared light beam is aimed at a dust particle are illustrated in Figure 2.1. Recalling the purpose of the LiDAR sensors in the mining environment, it is evident that

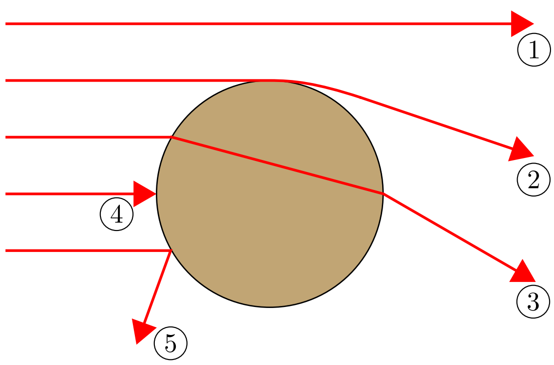

Figure 2.1: Scattering effects of light incident on dust: 1 no intersection; 2 diffraction; 3 refraction; 4 attenuation; and 5 reflection.

ideally there is no intersection with any dust particle at all. In the case of attenuation the sensor will not receive a return and is thus blinded by the dust (no information available). It is rather straightforward to determine if there is information available or not, but it may be difficult to apply a suitable control action. Diffraction, refraction, and reflection might lead to the conclusion that the object is somewhere else then where it actually is. As it is rather difficult to determine if the information is correct or not, diffraction, refraction, and reflection are extremely hazardous phenomena for automation purposes.

2.3 LD-LRS3100

The SICK LD-LRS3100 (Figure 2.2) is a long range 2D LiDAR sensor. In its output it returns the remission (in [%]) of the detected object. In the operating instructions [3] remission is described as the quality of reflection at a surface, with Table 2.1 presented as reference. As white paper was used as target wall (see subsection 3.2.5), the remission reported by the sensor should be close to 100% in clear conditions.

Figure 2.2: SICK LD-LRS3100.

Material	Remission
Black car paint, matt	5%
Black photographic cardboard, matt	10%
Grey concrete	18%
White cardboard	90%
White plaster	100%
Reflective film	$>$ 300%

Table 2.1: Typical remission values reported by the LD-LRS3100 according to Tab. 6 in [3].

2.4 LD-MRS

The SICK LD-MRS400102 (Figure 2.3) uses multi-layer and multi-echo technology, reports the pulse width of each of the echoes, and it classifies every measurement over three categories. It thus provides four additional information fields in its output: scan plane, echo number, pulse width, and flag. The long range tests required a different way of using the sensor than was done with the short range tests due to its wide beam divergence. The differences are listed in Table 2.2.

2.4.1 Multi-layer technology

The photo diode receiver of the LD-MRS consists of four independent receivers. This divides the aperture into scan planes creating four 2D scanning planes oriented $0.8°$ with respect to each other.

Figure 2.3: SICK LD-MRS400102.

Description	**Short range tests**	**Long range tests**
Mounting orientation	vertical	horizontal
Layer spread	horizontally	vertically
Beam divergence vertical	0.08°	0.8° (1))
Beam divergence horizontal	0.8° (1))	0.08°
Scanning frequency	$25Hz$	$12.5Hz$
Angular resolution mode	constant	focused
Angular resolution	0.2° (1)	0.125° (1)(3)
Reference figure in [4]	Fig. 3-13	Fig. 3-11

(1) Resolution between layers, see Fig. 3-5 and/or Tab. 9-1 in [4].
(2) Angular step between plane 1 or 2, and plane 3 or 4 (see Fig. 3-9 in [4]) The angular step on the same plane is twice as high.
(3) Central area only, i.e. ±10° from the central axis, see Fig. 3-11 in [4].

Table 2.2: The settings of the LD-MRS used for the long range tests differ from those used for the short range tests.

2.4.2 Multi-echo technology

The LD-MRS is capable of gathering three echoes per transmitted laser pulse. In the manual of the sensor [4] this technique is explained as follows. If a laser beam hits a glass pane, for example, a part of the light is reflected and triggers a measurement (echo 1). Most of the light passes the window pane and might hit a rain drop which then again reflects a part of the light (echo 2). The remaining light is then reflected by an object, which then results in the third measured value (echo 3).

2.4.3 Pulse width

The pulse width indicates how long the photo diode remains energised for that particular pulse. It is a duration which is transformed to a length by the LD-MRS using the speed of light,

2.4.4 Flags

The LD-MRS manual [4] states that the LD-MRS is able to classify if a measurement is valid, atmospheric noise (rain, dust, or similar), or contamination (dirt). However, the development team of the LD-MRS have recommended that the flag information field should be used solely to distinguish between valid and invalid returns.

2.5 LMS511

The SICK LMS511-10100 PRO (Figure 2.4) is a 2D scanner which, similar to the LD-MRS, uses multi-echo techniques (see also subsection 2.4.2). The PRO version is able to receive up to five echoes per transmitted laser pulse. The LMS511 reports an RSSI (Received Signal Strength Indicator) value for each measurement with 8-bit resolution. Table 2.3 gives the interpretation of these values.

Figure 2.4: SICK LMS511-10100 PRO.

RSSI value	Description
0	no signal
1-254	valid measurement
255	dazzled

Table 2.3: Interpretation of RSSI values reported by the LMS511 according to Tab. 10 in [2].

2.6 HDL-64E

The Velodyne HDL-64E S2 (Figure 2.5) evolved out of the DARPA Grand Challenge and is best known from its use in Google Street View imaging. It uses 64 emitter-detector pairs resulting in a vertical field of view from $-24.8°$ to $+2°$. Its output contains orientation, range, and intensity. The minimum and maximum intensity can be set using the calibration file and were set to 0 and 255, respectively (see also [5]).

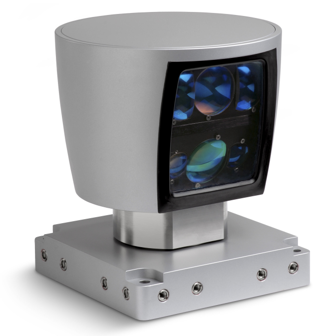

Figure 2.5: Velodyne HDL-64E S2.

Chapter 3

Experiments

In order to compare the four LiDAR sensors, an experimental setup was designed and realised at the CRCMining site of Pinjarra Hills in Queensland, Australia. The dust used in all of the long range tests is ISO 12103-1 A4 coarse test dust.

3.1 Purpose

The purpose of the experimental setup is to be able to qualify the behaviour of the four different LiDAR sensors with respect to dust clouds. The setup allows varying the dust cloud and the range.

It is assumed that the dust cloud can be solely characterised by the physical quantity transmittance. Transmittance is the fraction of incident light that passes through a certain medium. As it is a fraction, it is normally expressed as a percentage. When there is no interference with any medium other than the reference medium (here air) the transmittance equals 100%. When all the incident light is absorbed or scattered the transmittance equals 0%. The transmittance depends on the distance the beam travels through the volume of interest and is, for gasses, given by the Beer-Lambert law:

$$T = e^{-\alpha\delta},$$

where α is the attenuation coefficient (a material constant), and δ the path length. Both α and δ can be influenced: α by the amount of dust (the more dust, the higher the attenuation coefficient), and δ is one of the dimension parameters of the dust chamber (see also subsection 3.2.2). The method of measuring transmittance is explained in subsection 3.2.4.

3.2 Description experimental apparatus

An overview of the experimental apparatus is presented in Figure 3.1. A photograph of the experimental setup built at Pinjarra Hills is shown in Figure 3.2. In the following subsections the most important elements are discussed.

3.2.1 Creating dust clouds

In order to create dust clouds ten Ryobi RBL36B leaf blowers were used. These blowers were located on the side and spaced $0.5m$ apart (see also subsection 3.2.2). The blowers suck in air at the top of the chamber and blow it into trays at the bottom of the chamber. Due to the shape of the trays this causes the dust to go airborne. With a sufficient amount of dust in the chamber prior to turning on the blowers, the transmittance drops to 0% after the blowers are turned on. Turning the blowers off allows the dust to settle and hence the transmittance to slowly increase to 100%.

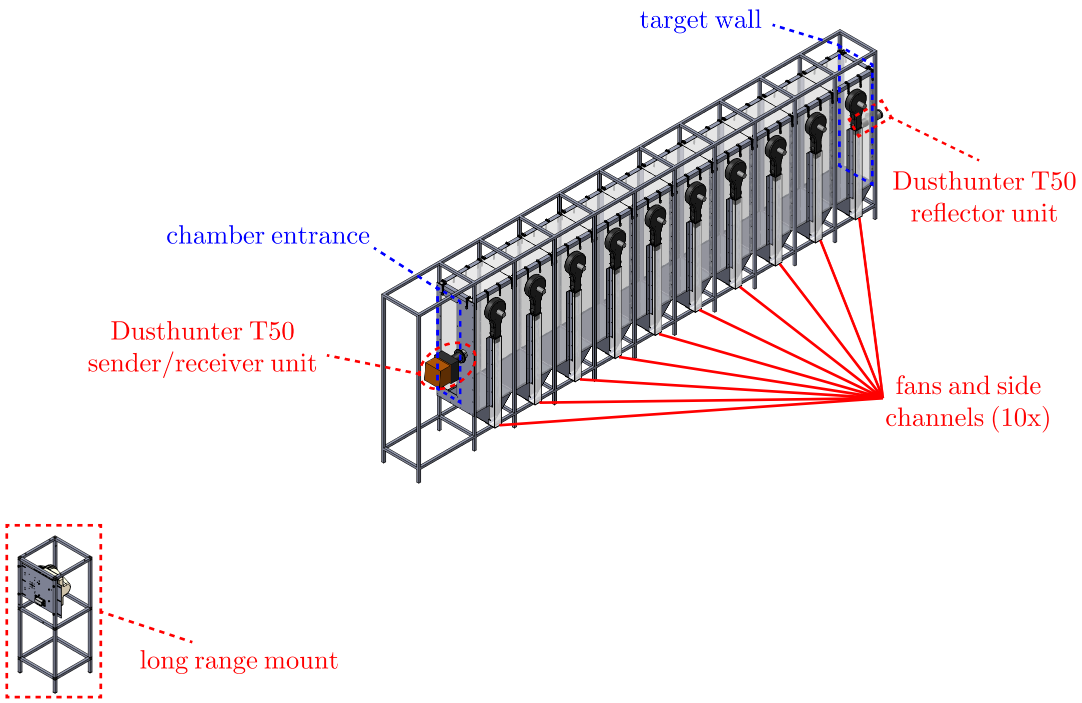

Figure 3.1: Schematic overview of the experimental setup.

3.2.2 Dimensioning

As dust settles, there is a gradient in the amount of dust in the vertical direction. Therefore, the LiDAR sensors and the transmittance monitor (see subsection 3.2.4) were installed at the same height. To keep the design compact it was decided to only test one of the LiDAR sensors at a time and to position the 2D sensors such that they scan in vertical direction. The width of the inside of the chamber is $0.4m$. In order to obtain a sufficient amount of returns from the target wall, the height of the target wall was set to $1.2m$. The most relevant dimensions are indicated in Figure 3.3.

3.2.3 Long range mount

For conducting tests with ranges varying from $10m$ to $25m$ (with a constant dust cloud width of $5m$), a separate mount was designed to support the LiDAR sensors. Figure 3.4 illustrates how the sensors were mounted on this long range mount. Recall that the LD-MRS is oriented horizontally instead of vertically as discussed in section 2.4.

3.2.4 Measuring transmittance

The transmittance was measured by use of a SICK Dusthunter T50. The sender/receiver unit of the Dusthunter T50 emits light in the visible $450 - 700nm$ range which is reflected back by the reflector unit. By measuring the amount of light that is returned and knowing the distance between the sender/receiver unit and the reflector unit, the device is able to determine the transmittance. The device also comes with a purge unit which prevents dust settling on both the sender/receiver unit and the reflector unit. The sender/receiver unit was mounted at the front of the chamber; the reflector unit was mounted on the target wall. The Dusthunter T50 requires calibration prior to measurements. The calibration includes setting the target distance, aligning the sender/receiver unit with the reflector unit, and setting 0% and 100% transmittance references.

Figure 3.2: Photograph of the experimental setup including the long range mount.

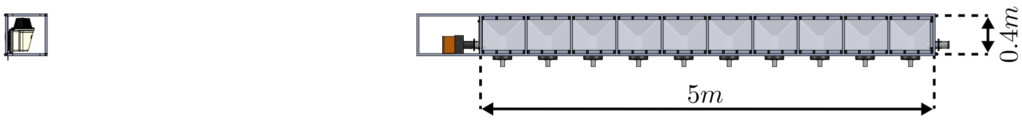

(a) Top view

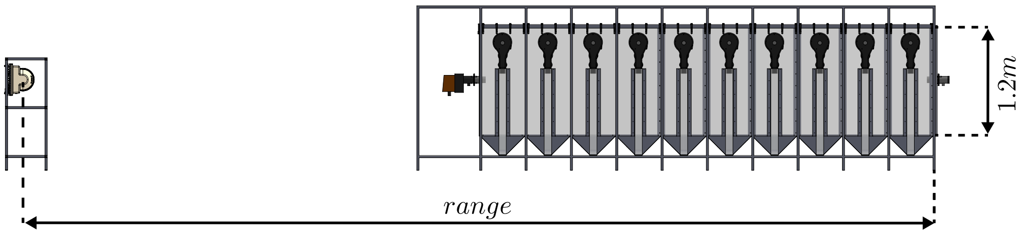

(b) Side view

Figure 3.3: Dimensions of the experimental setup with the LD-LRS3100 mounted on the long range mount on the left.

3.2.5 Walls

The walls are made out of transparent acrylic in order to allow for visual inspection. In addition to the acrylic, the target wall has sheets of white paper attached to it to create a non-transparent target for the LiDAR sensors. In the front wall there is a entrance on the sensor side for the LiDAR beam to enter the chamber, see also Figure 3.1. A reasonable amount of dust is lost through this entrance causing the transmittance to slowly increase even when the blowers are on.

3.2.6 Ambient light

Ambient light influences the transmittance measurements. Therefore, in order to create similar circumstances among all tests, an attempt was made to remove all ambient light near the dust cloud.

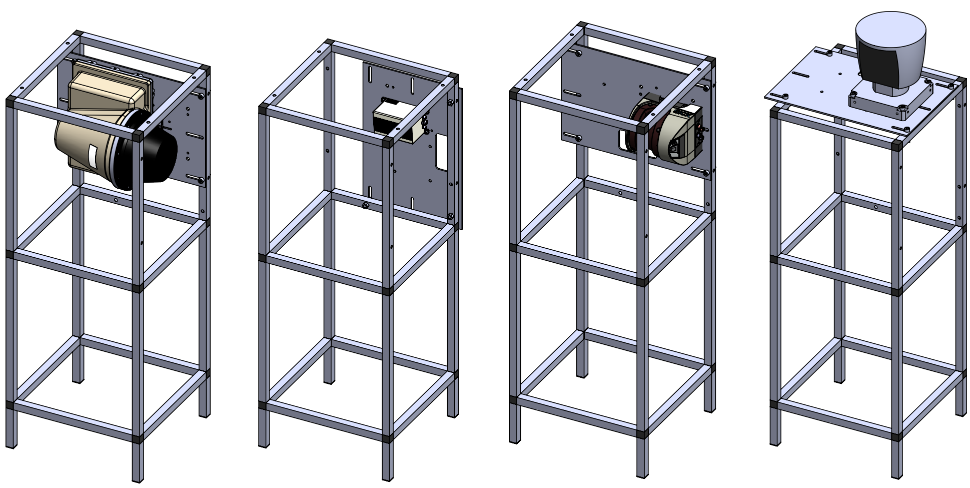

(a) LD-LRS3100 (b) LD-MRS (c) LMS511 (d) HDL-64E

Figure 3.4: Mounting positions of the four sensors on the long range mount.

3.3 Logging procedure

In this section the logging procedure that was used for all the tests is described based on the typical behaviour of the transmittance over time which is illustrated in Figure 3.5.

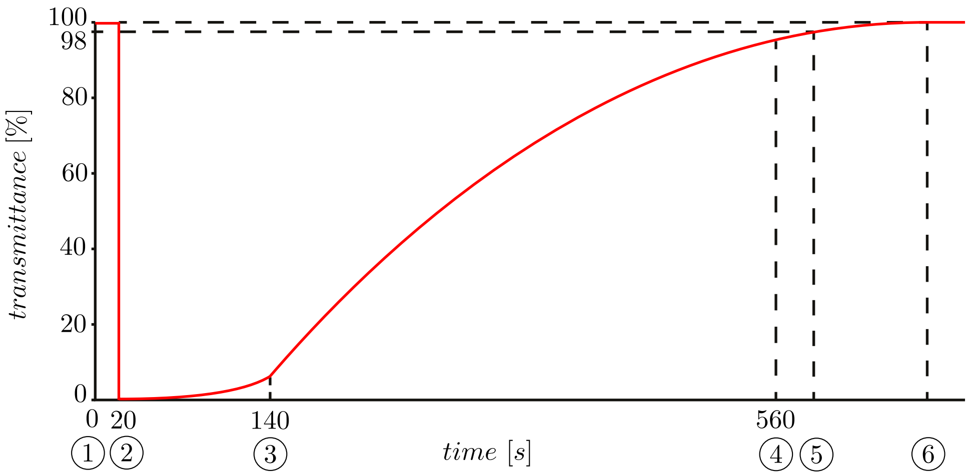

Figure 3.5: Typical behaviour of transmittance over time.

Before each test $40g$ of test dust was equally distributed in the chamber. The data of the Dusthunter T50 and the LiDAR sensor was logged on the same computer in order to keep the data synchronized. The monitoring of the data was done on a separate computer. The logging of each test was based on the characteristic points indicated in Figure 3.5 and performed as follows:

1. Start of logging when the transmittance is 98% or more.
2. The blowers are turned on after $20s$ in order to obtain sufficient clear conditions data. When turning on the blowers, the transmittance drops almost immediately to 0%. As dust can leave the chamber through the chamber entrance, the transmittance starts to slowly increase.
3. The blowers are turned off after they have been on for two minutes, i.e. after $140s$. With the blowers being turned off, the dust is able to settle and the transmittance increases more rapidly.
4. The logging is stopped seven minutes after the blowers were turned off, i.e. after $560s$. The next test is prepared by adding dust to the chamber and cleaning the lens of the sensor.
5. The transmittance becomes 98% or more and the procedure can be repeated from step 1.
6. If the blowers are not turned on, the transmittance will eventually reach 100%.

Chapter 4

Results

In this chapter the results of the executed tests are presented and discussed for each of the four sensors.

All four sensors showed similar behaviour for each range in contrast to the short range tests. In clear conditions the sensor reported the target wall. After the blowers were turned on, there were spurious returns mapping the front of the dust cloud. After a while the sensor was completely blinded and there were no returns. As transmittance increased, the target wall was reported again and became more visible as transmittance increased (i.e. with increasing remission, pulse width, RSSI, or intensity).

4.1 Data presented

Occasionally, there was lag present in the data provided by the Dusthunter T50 resulting in a zero-order hold being applied. See, for example, Figure 4.1 which shows one of the transmittance curves measured during the tests. As the behaviour of the sensors is characterised by the transmittance value, the effect of the zero-order hold on the results is significant when the transmittance changes rapidly, i.e. when the blowers were turned on. As the blowers were turned on around $20s$, only the data logged in the first $15s$ and after $25s$ is presented. During the first $15s$ the transmittance is approximately 100% and this data can be used as reference for clear conditions. For each sensor, an area on the target wall was determined from which range measurements could be seen in clear conditions.

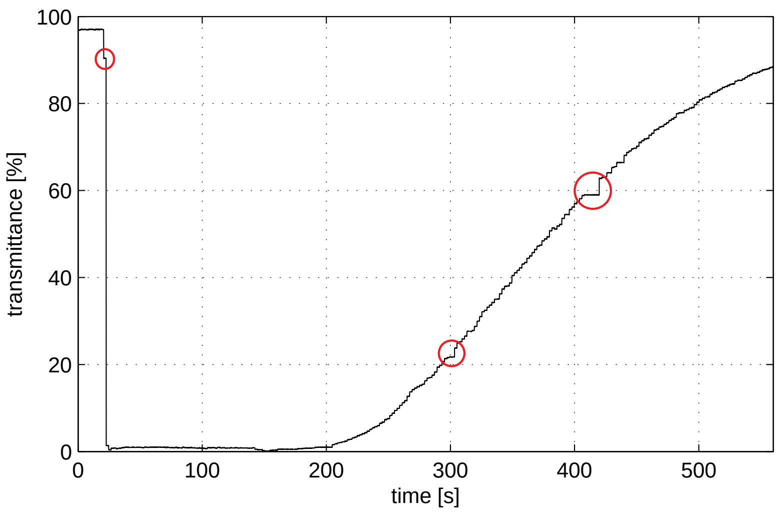

Figure 4.1: When there is no data available, the Dusthunter T50 applies a zero-order-hold (red circles) which, when occurring during the drop, would significantly affect the results.

Measurements corresponding with low transmittance values contain the most dynamic, and thus the most interesting, behaviour. Therefore, the results presented are collected in twenty transmittance intervals on a logarithmic scale. Error bars indicate one time the standard deviation.

4.2 LD-LRS3100

Figure 4.2 depicts the remission as reported by the LD-LRS3100 in clear conditions. Contrary to the short range tests, there is backscatter observed as the dust cloud is further away than the minimum range of $2.5m$ [3]. Note, however, that the LD-LRS3100 did report returns at distances as close as $2m$. The data that is presented consists of measurements aimed between $\pm 0.4m$ in y-direction on the target wall as illustrated by the magenta area in Figure 4.2.

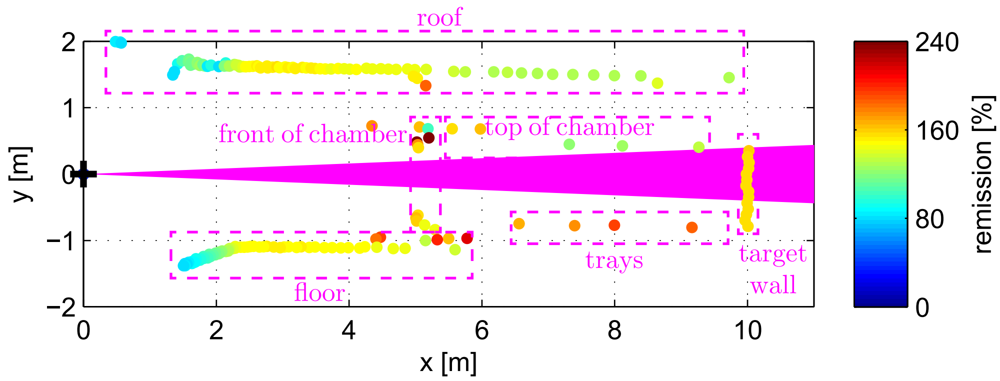

Figure 4.2: Remission reported by the LD-LRS3100 for a scan in clear conditions at $10m$ range. Only measurements inside the magenta area are presented.

For the $20m$ range tests the three tests seem to be inconsistent resulting in large variances. For the $25m$ range test, test 1 is inconsistent with test 2 and test 3.

4.2.1 Number of returns

Figure 4.3 shows the number of returns for each measured transmittance value. As there is a period in which the sensor is blinded (i.e. there are no returns) corresponding to a low transmittance, the number of returns per scan is low for low transmittance values. For all ranges the same angular resolution of $0.5°$ was used. Therefore, there are on average more returns of the target wall per scan for shorter ranges than for longer ranges.

4.2.2 Distance

Figure 4.4 shows the horizontal distance reported by the sensor. Once the sensor observes the target wall, the reported distance is close to the distance reported in clear conditions (within a centimetre).

4.2.3 Remission

The remission should be approximately 100% in clear conditions according to the manual [4] as white paper was used on the target wall. However, the reported values are considerably larger for all ranges. For the $10m$, $15m$, $20m$, and $25m$ range tests the mean reported remissions in clear conditions were 157%, 169%, 173%, and 176%, respectively. Instead, the dust cloud (observed for low transmittance values) is reported to have a remission close to 100% as can be seen in Figure 4.5.

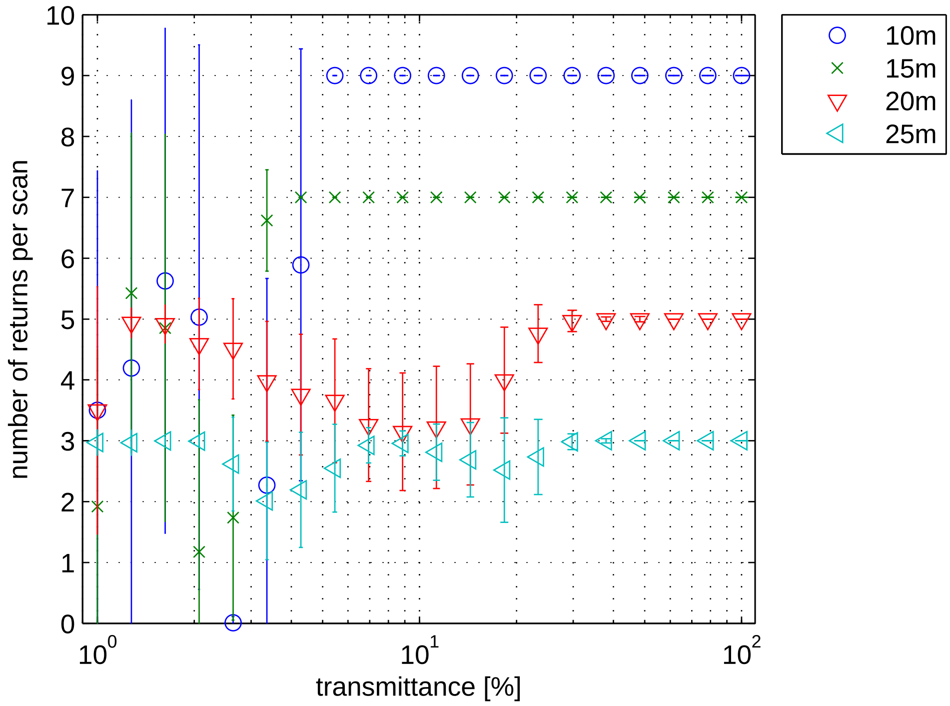

Figure 4.3: Number of returns reported by the LD-LRS3100.

4.2.4 Summary

The dust cloud is observed with less returns and a lower remission at low transmittance values. The reported remission of the target wall increases when the transmittance increases whereas the number of returns from, and the position of, the target wall are unaffected when the transmittance changed. Instead of the target wall (which was reported with a remission of approximately 170%), the front of the dust cloud was reported with a transmission close to 100%.

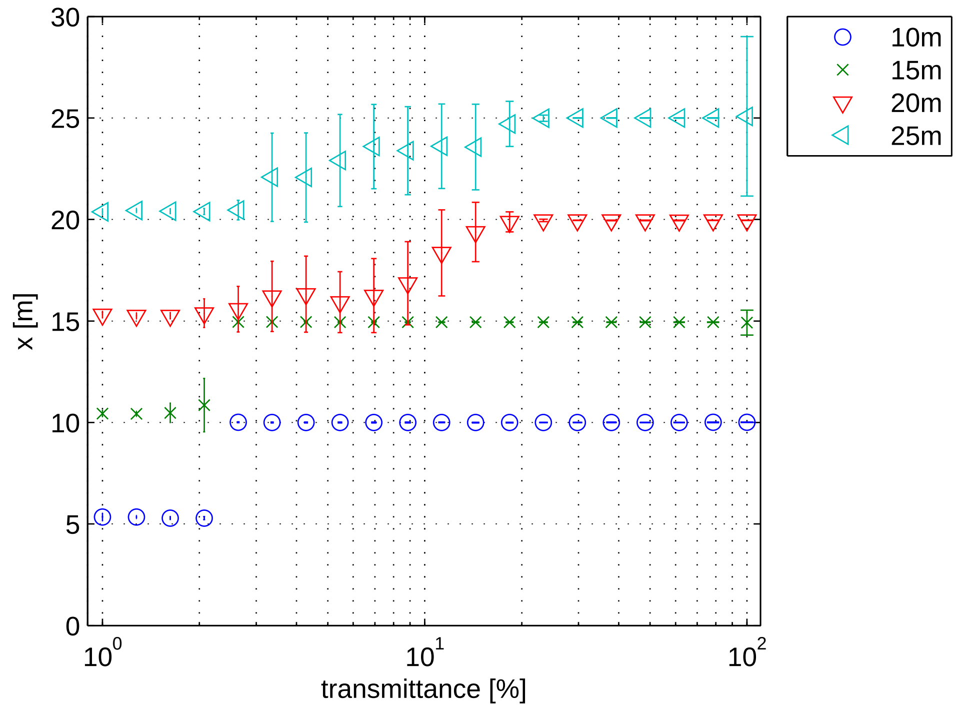

Figure 4.4: Horizontal distance x reported by the LD-LRS3100.

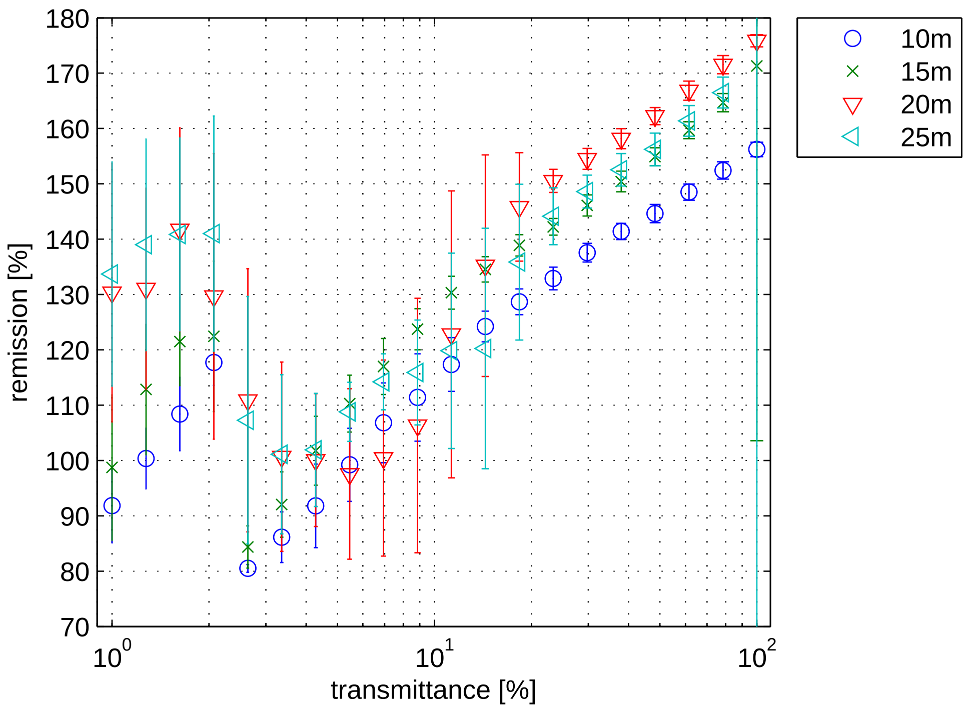

Figure 4.5: Remission reported by the LD-LRS3100.

4.3 LD-MRS

The pulse width of returns as reported by the LD-MRS for one of the $10m$ range tests in clear conditions is shown in Figure 4.6.

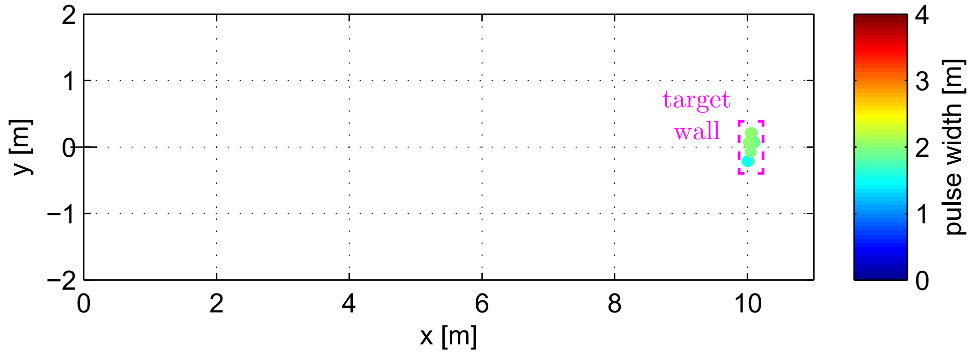

Figure 4.6: Pulse width reported by the LD-MRS for a scan in clear conditions at $10m$ range.

The data that is presented consists of measurements aimed at the target wall between $\pm 0.5m$ in vertical (y) and $\pm 0.05m$ in horizontal (z) direction as illustrated by the magenta area in Figure 4.7 for the $10m$ range tests.

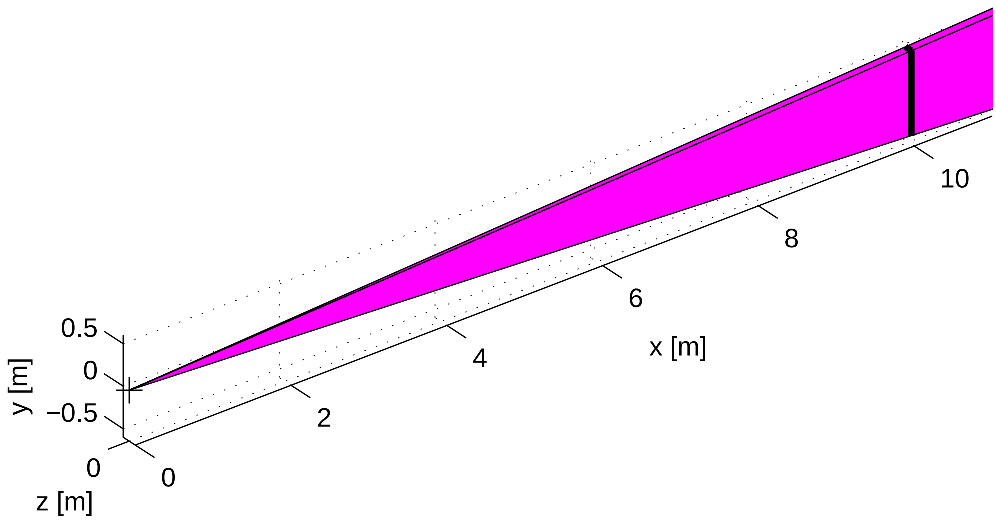

Figure 4.7: Only measurements inside the magenta area are presented for the LD-MRS.

4.3.1 Distance

The estimate of the horizontal distance x appears to be more consistent across the three tests for longer ranges, see Figure 4.8.

4.3.2 Pulse width

The pulse width reported by the LD-MRS is shown in Figure 4.9. The average pulse width reported is the same for the different ranges for high transmittance values although the variance on it is larger for the shorter ranges. For low transmittance values the sensor reports a larger pulse width on the $10m$ range tests and a smaller pulse width on the $20m$ and $25m$ range tests than in clear conditions.

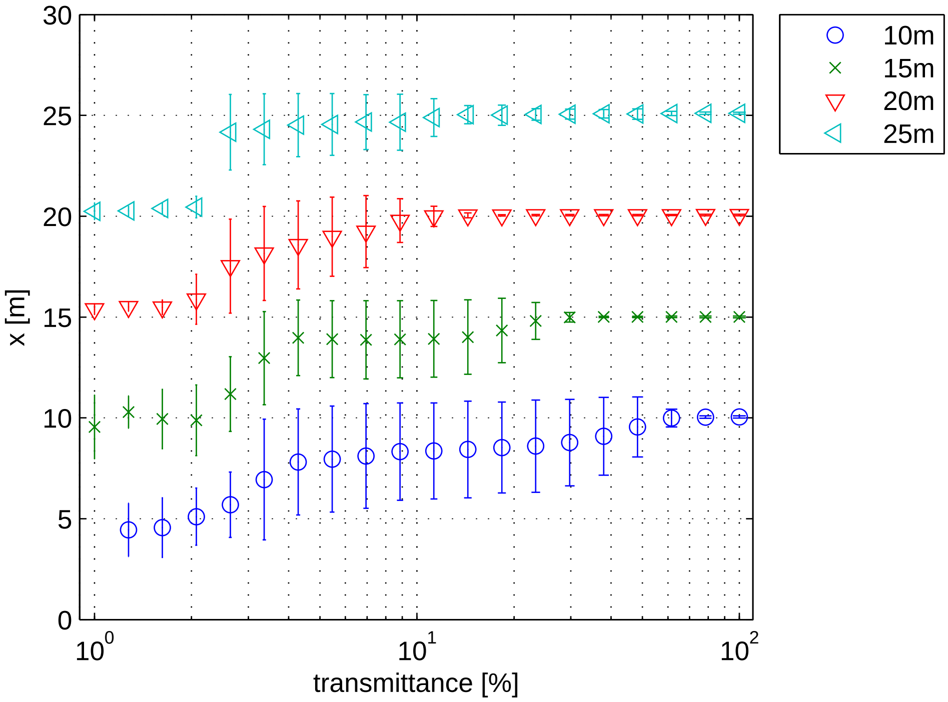

Figure 4.8: Horizontal distance x reported by the LD-MRS.

4.3.3 Echo

The LD-MRS reported up to all possible three echoes as is shown in Figure 4.10. In Figure 4.11 the measurements in the yz-plane are shown in clear conditions per layer as reference.

4.3.4 Flag

The ability of the LD-MRS to classify returns as valid or invalid is illustrated in Figure 4.12 per transmittance interval. In Figure 4.13 the percentage of returns classified as valid is shown as function of the horizontal distance x. The figure shows that returns from the target wall are in general all classified as valid whereas returns from the dust cloud ($5m$ closer than the range) were more often classified as invalid. There is, however, still a considerable amount of returns from the dust cloud being classified as valid.

4.3.5 Summary

The behaviour of the LD-MRS is similar to the behaviour of the other sensors. The sensor occasionally classifies returns from dust as invalid measurements. However, there was also a significant number of returns from dust which were classified as valid. The ability of the LD-MRS to classify returns as valid or invalid is thus insufficient to distinguish between the target wall and the dust cloud.

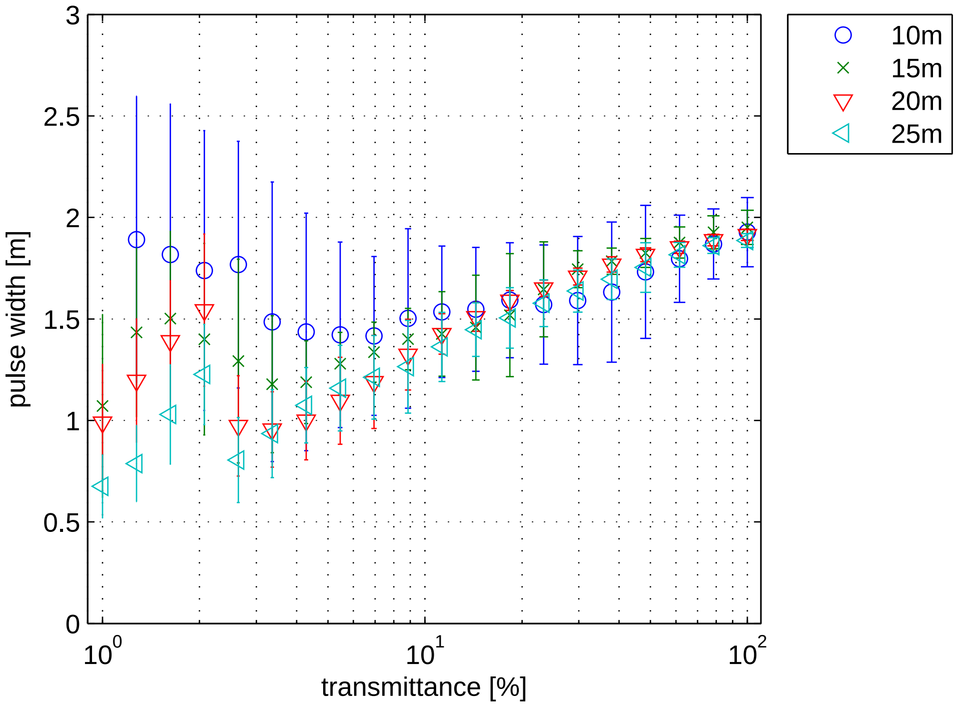

Figure 4.9: Pulse width reported by the LD-MRS.

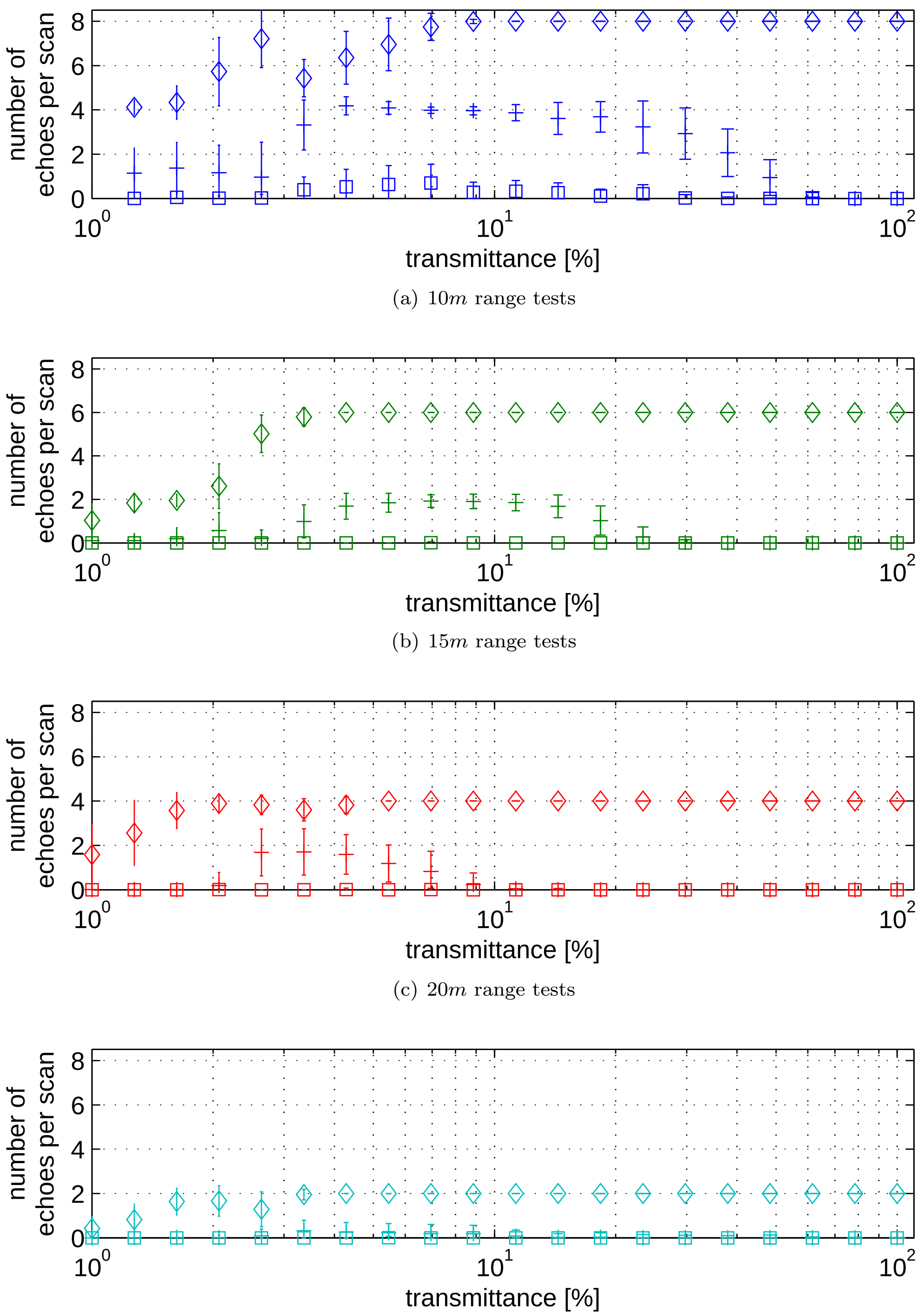

(a) $10m$ range tests

(b) $15m$ range tests

(c) $20m$ range tests

(d) $25m$ range tests

Figure 4.10: Number of echoes per scan as reported by the LD-MRS. First echoes (diamonds), second echoes (plus), and third echoes (squares) were reported.

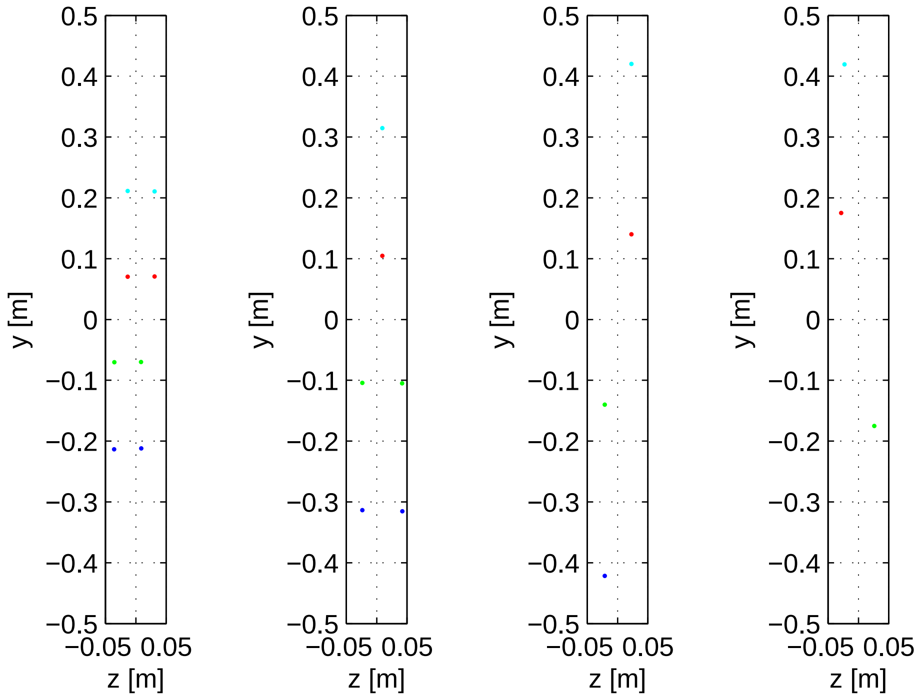

(a) 10m range tests (b) 15m range tests (c) 20m range tests (d) 25m range tests

Figure 4.11: Measurements in clear conditions on the first (blue), second (green), third (red), and fourth (cyan) layer in yz-plane. The measurement on the fourth layer for the 25m tests was at $x \approx 20$ and hence not in the considered region.

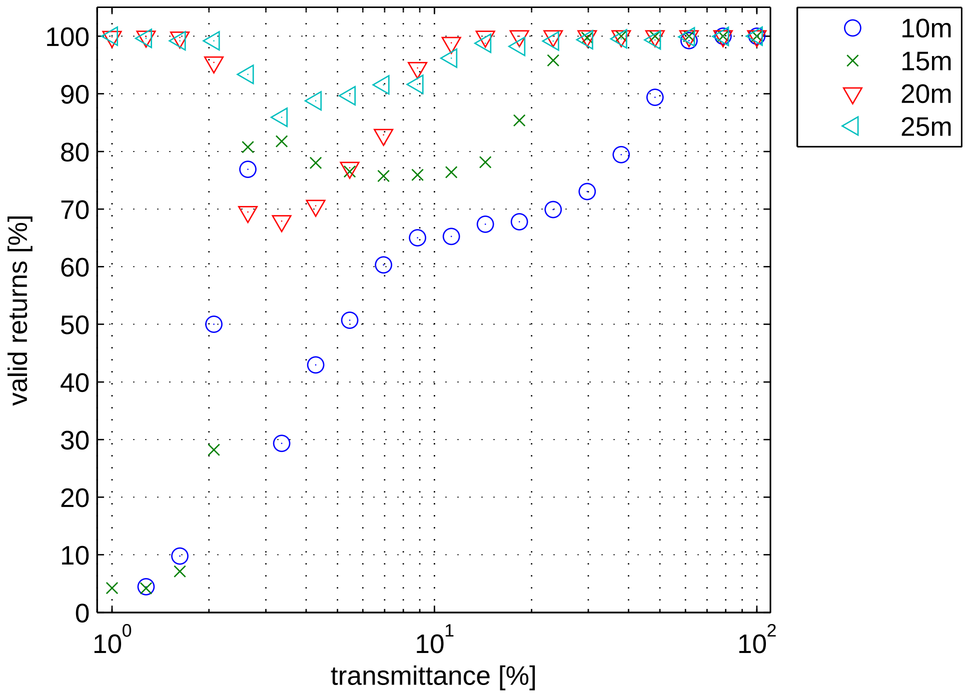

Figure 4.12: The higher the transmittance, the more often returns were classified as valid.

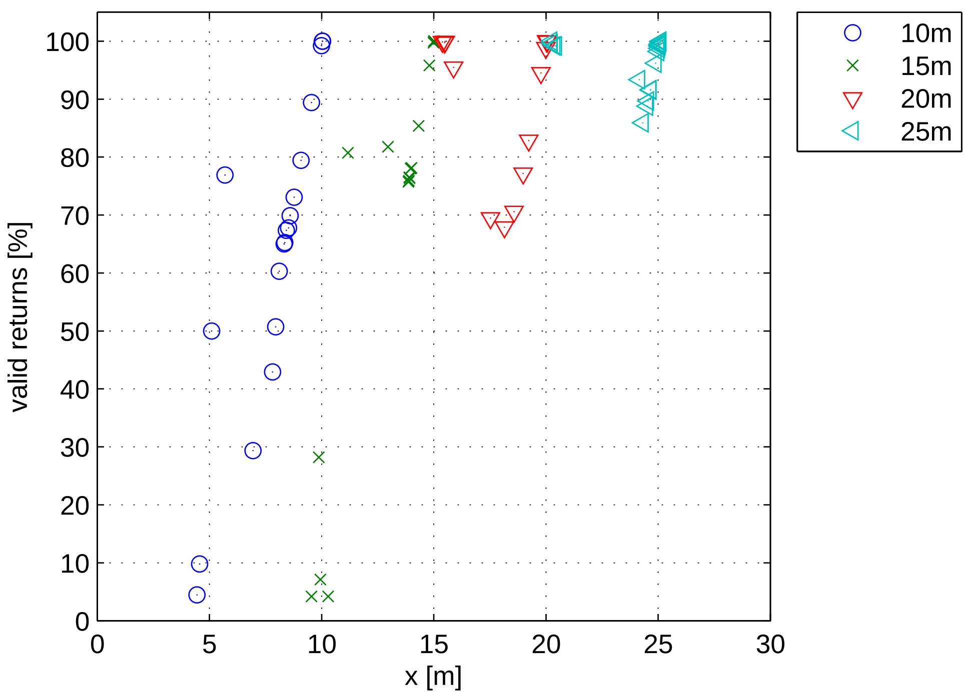

Figure 4.13: Returns reported further away were more often classified as valid.

4.4 LMS511

Figure 4.14 depicts the RSSI values reported in clear conditions for one of the $10m$ range tests with the LMS511. The data that is presented consists of measurements aimed between $\pm 0.5m$ on the target wall as illustrated by the magenta area in Figure 4.14.

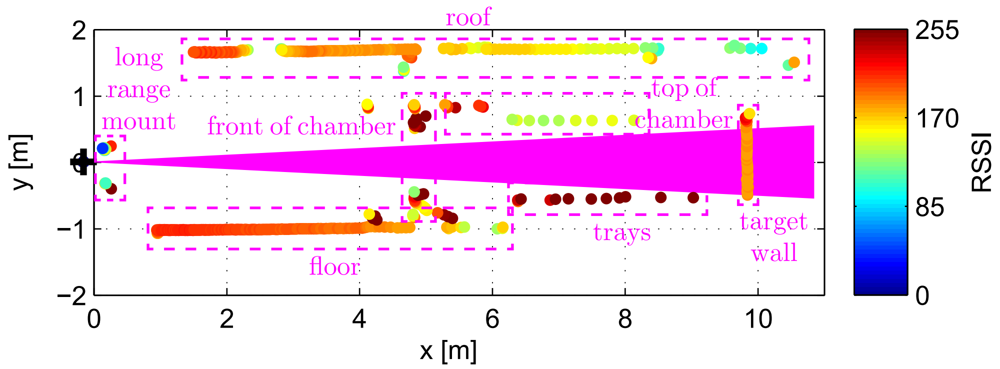

Figure 4.14: RSSI reported by the LMS511 for a scan in clear conditions at $10m$ range. Only measurements inside the magenta area are presented.

4.4.1 Distance

In Figure 4.15 the horizontal distance x reported by the LMS511 is shown for the four different ranges. The LMS511 shows consistent behaviour in the reported distance among these ranges.

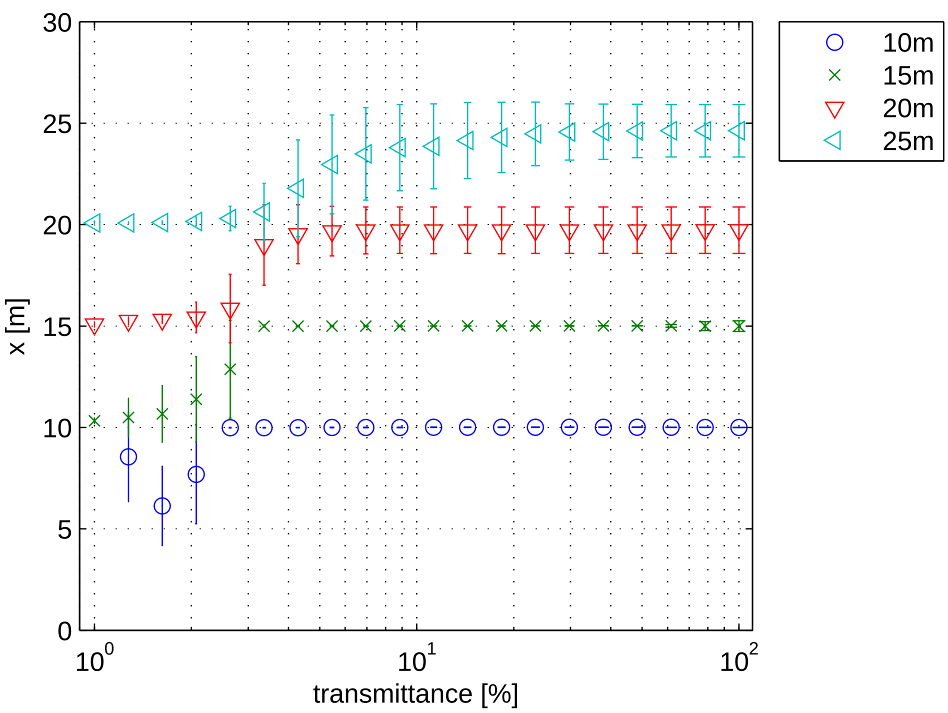

Figure 4.15: Horizontal distance x reported by the LMS511.

4.4.2 RSSI

A RSSI value of 0, indicating that the sensor did not receive a signal, was never reported. The sensor also never reported to be dazzled, i.e. it never reported a RSSI value of 255. See also Table 2.3. Figure 4.16 shows the RSSI values that were reported.

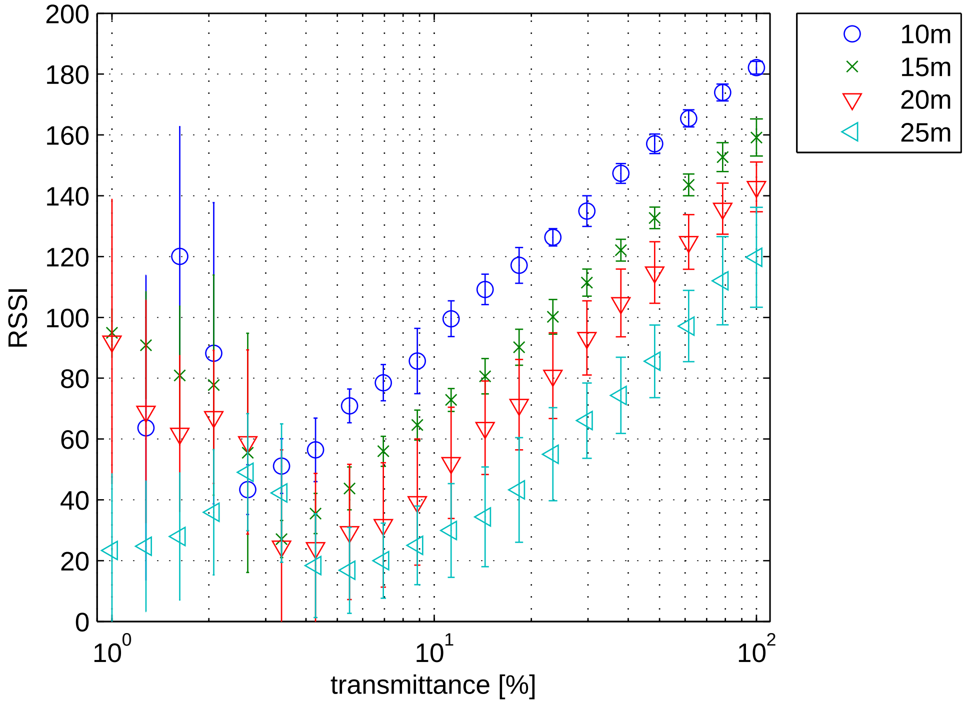

Figure 4.16: RSSI reported by the LMS511.

4.4.3 Echo

In contrast to the LD-MRS (which reported up to three echoes), the LMS511 only reported first and second echoes out of the possible five echoes. Figure 4.17 shows the number of echoes per scan. The number of second echoes seems to increase as the range increases. No second echoes were reported for the $10m$ range tests.

4.4.4 Summary

The LMS511 never reported to have no signal or to be dazzled during all of the long range tests. Only first and second echoes were reported.

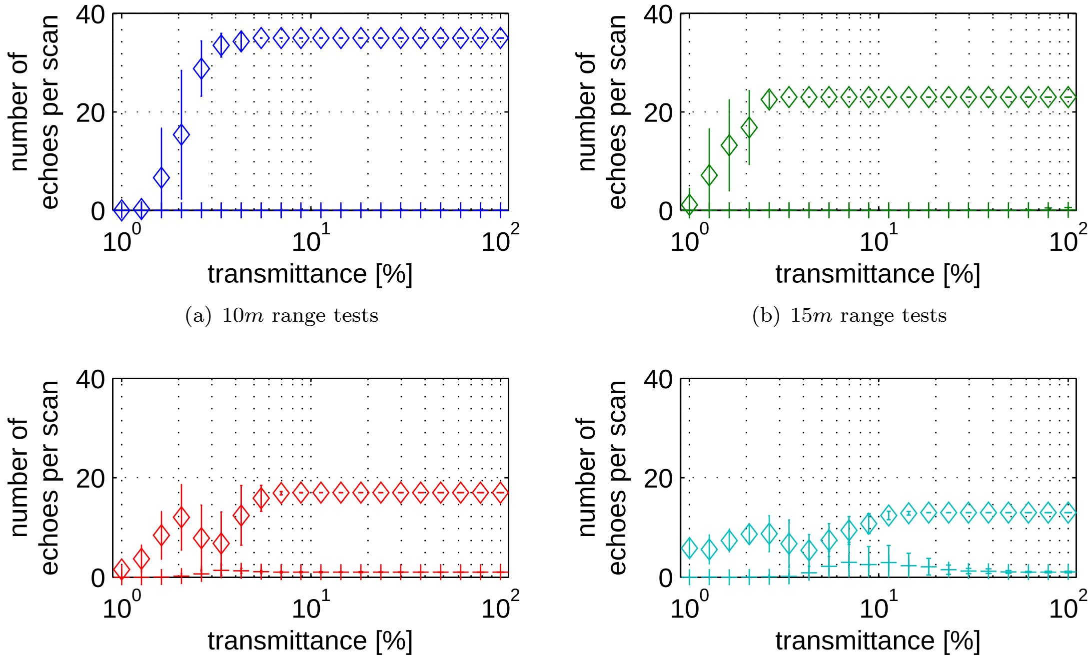

(a) $10m$ range tests (b) $15m$ range tests

(c) $20m$ range tests (d) $25m$ range tests

Figure 4.17: Number of echoes per scan as reported by the LMS511. Only first echoes (diamonds) and second echoes (plus) were reported.

4.5 HDL-64E

For presenting the results it is convenient to have the co-ordinate frame of the sensor coincident with the co-ordinate frame of the dust chamber. However, there was always a (small) mismatch between the two frames for the tests with the HDL-64E as is illustrated in Figure 4.18. The black co-ordinate frame is the reference frame, the red co-ordinate frame is the sensor's co-ordinate frame, and the blue co-ordinate frame is the rotated version of the red frame such that its x-axis is aimed at the middle of the chamber entrance. By using markers on the floor, it was possible to keep the translational mismatches Δx and Δy small. However, it was difficult to obtain a small angular mismatch β using the HDL-64E viewer. Assuming $\Delta x \approx \Delta y \approx 0$ it follows that $\gamma \approx 0$, and thus that $\alpha \approx \beta$ is the only mismatch. For each range a correction on α was determined such that β was acceptably small.

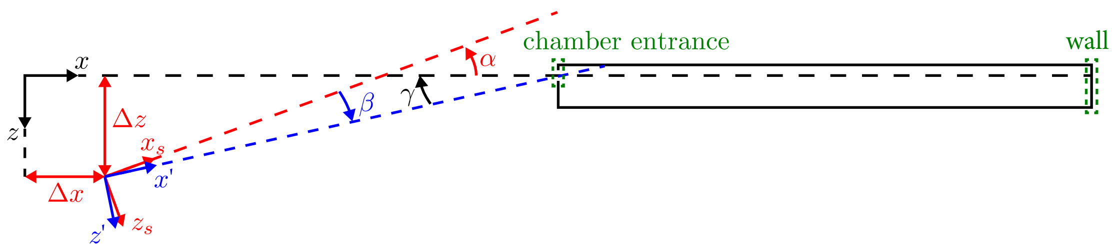

Figure 4.18: Top view illustrating the mismatch between the co-ordinate frames for the HDL-64E. A correction was applied for the rotational mismatch α.

With the factory calibration parameters, the HDL-64E has shown to be poorly calibrated. For example, a flat wall at $10m$ distance was reported with variations up to $10cm$. See also Figure 4.19. In contrast to the other three sensors, the HDL-64E has two emitter blocks which are located $134mm$

and 207mm above the sensor's origin and a non-symmetric vertical field of view.

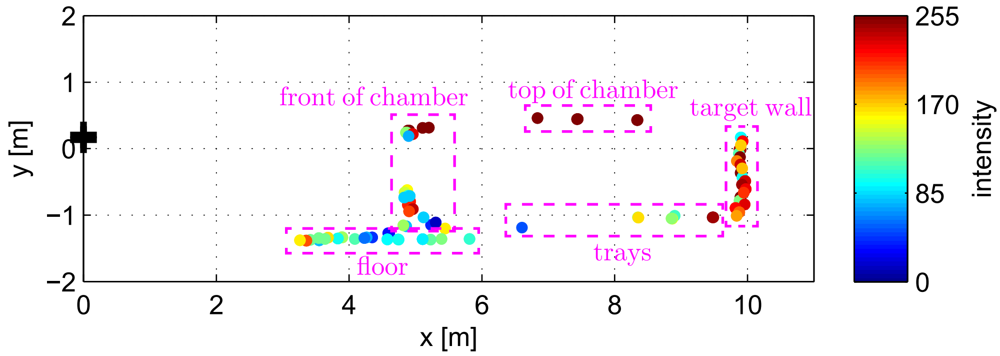

Figure 4.19: Intensity reported by the HDL-64E for a scan in clear conditions at 10m range.

Recalibrating the HDL-64E is part of current research. The calibration parameters are used to transform the collected data to Cartesian co-ordinates which allows for reanalysis with the correct values without redoing the experiments. At the moment of writing this report there was no better set of calibration parameters available than the factory set which was therefore used. As these calibration parameters only induce mismatches in the order of centimetres for the position of the returns but not affected the reported intensity, the main conclusions of the analysis will remain unchanged when the analysis is redone using better calibration parameters. However, the poorly calibrated sensor only allowed to use measurements aimed at $\pm 5mm$, $\pm 4mm$, and $\pm 3mm$ in z-direction on the target wall (after the angular correction is applied) for the 10m, 15m, and 20m range tests, respectively. The third 25m range test had only a very small number of measurements that were aimed at the target wall. Therefore, only the first and second test of the 25m range tests with the HDL-64E are presented which allowed to use measurements aimed at $\pm 8mm$ on the target wall in z-direction. For all ranges only measurements aimed at the target wall between $+0.2m$ and $-0.8m$ in vertical (y) direction are presented. The data that is presented is indicated for the 10m range tests by the magenta area in Figure 4.20.

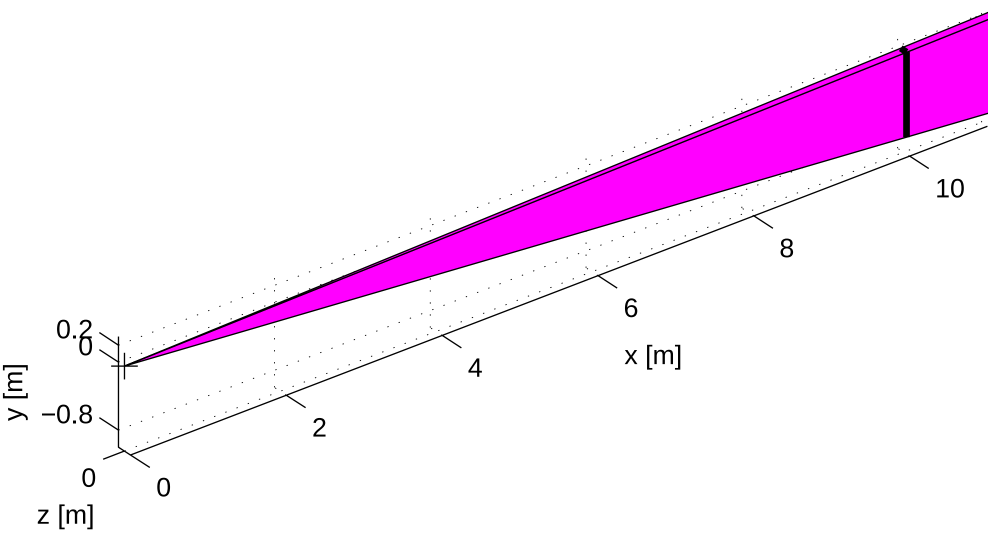

Figure 4.20: Only measurements inside the magenta area are presented for the HDL-64E.

4.5.1 Number of returns

Due to the poor calibration, the variance on the number of returns is even significant for high transmittance values, see Figure 4.21.

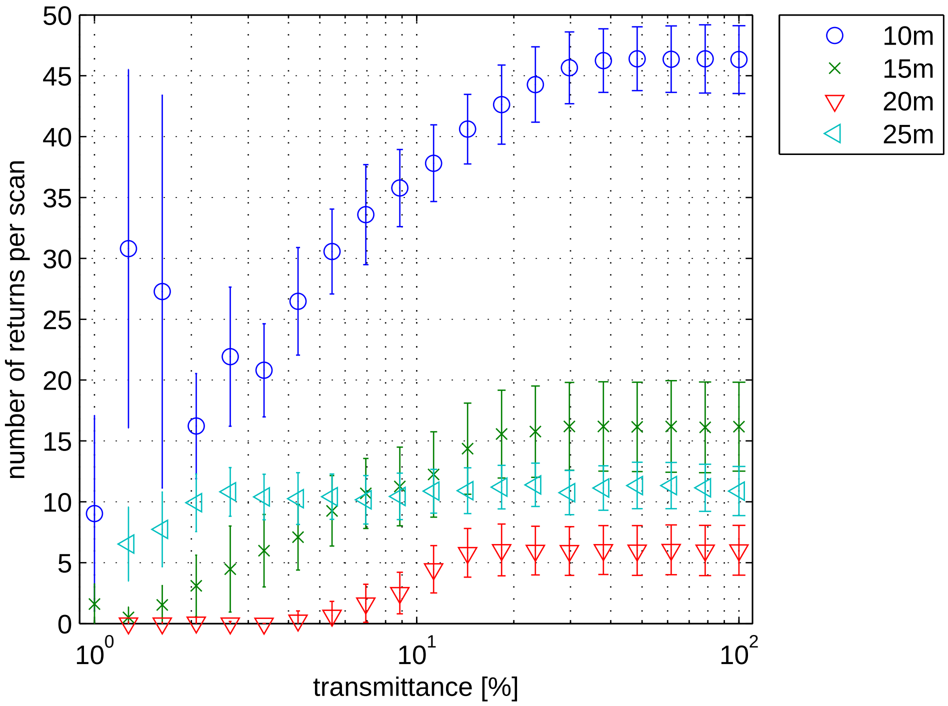

Figure 4.21: Number of returns reported by the HDL-64E.

4.5.2 Distance

The reported distance is presented in Figure 4.22 and shows typical behaviour.

4.5.3 Intensity

Figure 4.23 shows the intensity values that were reported which come with large variation.

4.5.4 Summary

Due to the poor calibration of the HDL-64E and the difficulties in aligning the sensor, the third $25m$ range test of the HDL-64E was omitted. The tests that are presented show behaviour similar to the other sensors but with relatively large variance.

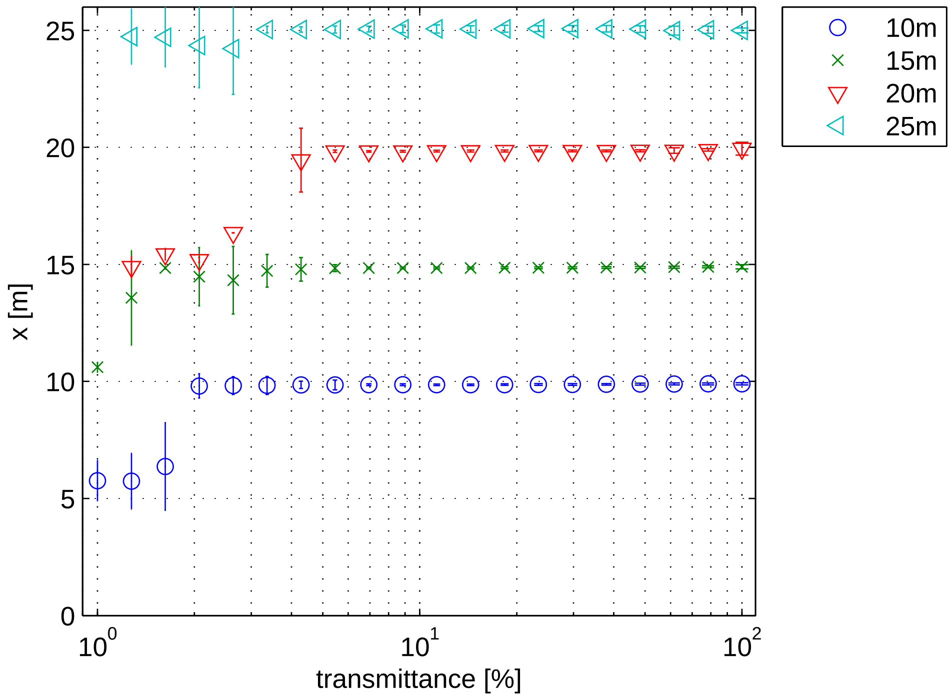

Figure 4.22: Horizontal distance x for all three tests per range.

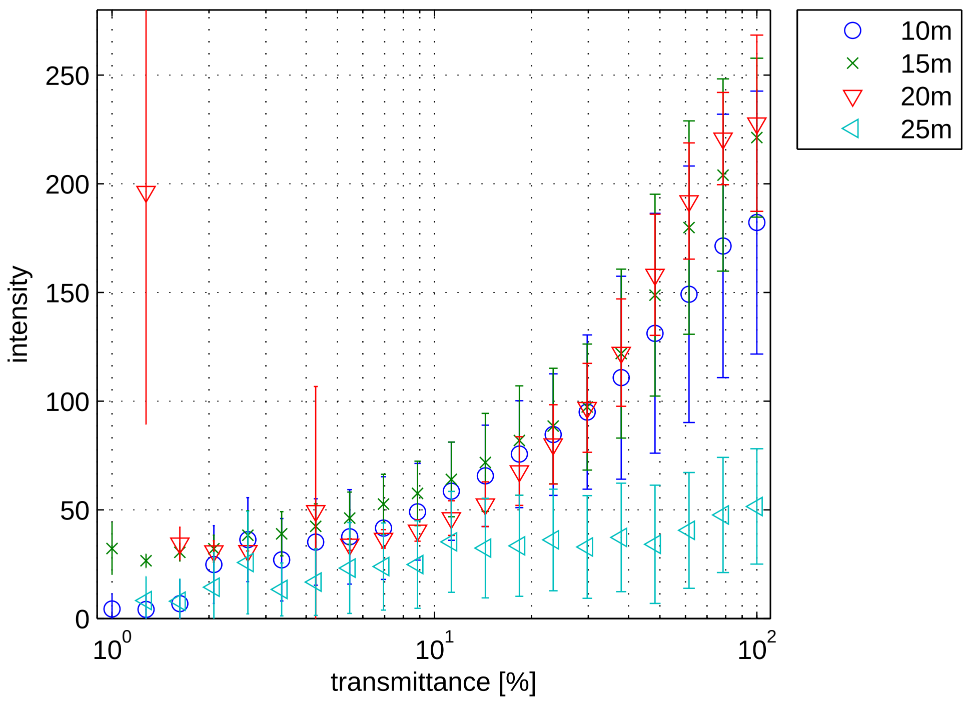

Figure 4.23: Intensity for all three tests per range.

Chapter 5

Recommendations for future research

What follows is a list of recommendations for future research.

- Based on the physics, different types of dust (for example different particle size or different distributions) would yield different results. One would prefer to conduct experiments with dust typically encountered in mining environments.
- Only one particular type of target (flat wall with white paper) was used while a lot of different objects are to be detected at a mining site. It would be interesting to study the effect of changing the properties of the target wall. For example, colour, reflectivity, surface roughness, geometry (e.g. spherical), and orientation (e.g. non-perpendicular surfaces).
- A limited attempt has been made to remove the ambient light in order to create similar circumstances for each test. It is, however, not feasible to remove the ambient light at a mining site and it is thus required to investigate the effect (if any) of ambient light on the results.
- In this study a certain method of creating dust clouds is chosen. It is, however, not evaluated if this is a reliable and suitable method. It is, for example, not verified if the dust cloud is uniform in the width direction of the chamber which could possibly result in density differences in horizontal direction. That is, the transmittance of the dust cloud at which the LiDAR sensor is aimed might be different from the transmittance of the dust cloud the Dusthunter T50 measures.
- In this study the dust cloud is characterised by a transmittance value only which might be too much of a simplification. A dimension which seems to be interesting to know is the density of the dust cloud, i.e. weight per volume. Also other devices for measuring transmittance should be considered for verification purposes.
- In order to rely less on the transmittance measurement for comparing sensors, one might log all the LiDAR sensors at the same time. This would, however, require that the dust cloud is uniform in at least one direction. Moreover, there should be no interference between the different sensors.
- The on-board processing of raw signals is unique between sensors. The raw signal on the photodetector would need to be analysed to truly identify how dust influences the determination of range measurements.
- Currently, the study is limited to tests on an experimental setup. One would like to compare this data with data resulting from tests conducted in actual mining environments in order to verify if the experimental setup is a accurate representation of reality.

Bibliography

[1] Tyson Phillips, Jurgen van Zundert, and Ross McAree. Perception sensor capabilities - phase 2, part b. Technical report, CRCMining, August 2013.

[2] SICK AG Waldkirch, Auto Ident, Reute Plant, Nimburger Strasse 11, 79276 Reute, Germany. *Laser Measurement Sensors of the LMS5xx Product Family*, 2012-04-28 edition.

[3] SICK AG Waldkirch, Auto Ident, Reute Plant, Nimburger Strasse 11, 79276 Reute, Germany. *LD-LRS1000 to 5100 Laser Measurement System*, 2008-05-30 edition.

[4] SICK AG Waldkirch, Auto Ident, Reute Plant, Nimburger Strasse 11, 79276 Reute, Germany. *LD-MRS Laser Measurement Sensor*, 2011-04-12 edition.

[5] Velodyne LIDAR, Inc., 345 Digital Drive, Morgan Hill, CA 95037. *User's manual and programming guide HDL-64E S2 and S2.1*, firmware version 4.07 edition.